sensitive indicators. The use of infrared absorption measured through the evanescent waves in optical fibers for sub-sea monitoring of organic compounds (at parts per million levels) has also been demonstrated. However, there is substantial interest in new sensors for oceanographic applications including monitoring of nutrients and pollutants, and optical sensors have great potential here. The devices are clearly attractive in concept and require expertise from several scientific disciplines including analytical chemistry, polymer chemistry, environmental chemistry, fiber-optics and opto-electronics.

See also

Fluorometry for Chemical Sensing. Inherent Optical Properties and Irradiance. Wet Chemical Analysers.

Further Reading

Hales B, Burgess L and Emerson S (1997) An absorbance-based fiber-optic sensor for CO_2(aq) measurement in pure waters of sea floor sediments. *Marine Chemistry* 59: 51–62.

Harmer AL and Narayanaswamy R (1988) Spectroscopic and fibre-optic transducers, In: Edmunds TE (ed.) *Chemical Sensors*. Glasgow: Blackie.

Mizaikoff B (1999) Mid-infrared evanescent wave sensors – a novel approach for sub-sea monitoring. *Measurement Science and Technology* 10: 1185–1194.

Narayanaswamy R (1991), Current developments in optical biochemical sensors *Biosensors and Bioelectronics*, 6: 467–475.

Narayanaswamy R (1993) Optical chemical sensors: Transduction and signal processing. *Analyst* 118: 317–322

Narayanaswamy R (1993) Chemical transducers based on fibre optics for environmental monitoring. *The Science of the Total Environment* 135: 103–113.

Narayanaswamy R and Sevilla FS III (1988) Optical fibre sensors for chemical species. *Journal of Physics E: Scientific Instruments* 21: 10–17.

Oehme I and Wolfbeis OS (1997) Optical sensors for determination of heavy metal ions. *Microchimica Acta* 126: 177–192.

Rogers KR and Poziomek EJ (1996) Fiber optic sensors for environmental monitoring. *Chemosphere* 33: 1151–1174.

Seitz WR (1988) Chemical sensors based on immobilised indicators and fiber optics. *CRC Critical Reviews in Analytical Chemistry* 19: 135–171.

Tokar JM and Dickey TDN (2000) Chemical sensor technology. Current and future applications. *Ocean Science and Technology* 1: 303–329.

Wise DL and Wingard LB Jr (1991) *Biosensors with Fiberoptics*. Clifton, NJ: Humana Press.

Wolfbeis OS (1991), *Fiber Optic Chemical Sensors and Biosensors*, 2 vols. Boca Raton, FL: CRC Press.

ABYSSAL CURRENTS

W. Zenk, Universität Kiel, Kiel, Germany

doi:10.1006/rwos.2001.0362

Introduction

Historically the term 'abyss' characterizes the dark, apparently bottomless ocean under extreme static pressure far beyond coastal and shelf areas. Today this ancient definition remains still rather unfocused in earth sciences. Geographers, marine biologists, and geologists use abyss for deep-sea regions with water depths exceeding 1000 or 4000 m. In physical oceanography a widely accepted definition of the abyss denotes the water column that ranges from the base of the main thermocline down to the seabed.

The main thermocline itself – occasionally also called warm-water sphere – extends laterally between the polar frontal zones of both hemispheres. In contrast to deep strata the surface exposition of the thermocline allows the direct exchange of heat, substances, and kinetic energy with the atmosphere. This wind-driven part of the water column and its fluctuations are consequently an immediate subject of weather and climatic conditions. The base of the thermocline at about 1000–1200 m represents the lower boundary of the warm-water sphere with temperatures well $>5^{\circ}$C.

The abyss or cold-water sphere below, is clearly colder. Below 2000 m potential temperatures $<4^{\circ}$C are found virtually everywhere. Below 4000 m values of 0–2°C are more characteristic. Until the advent of modern self-recording instrumentation abyssal currents were believed to be very slow ($<2\,\mathrm{cm\,s^{-1}}$) and negligible in comparison with rather vigorous and variable surface currents (sometimes $>100\,\mathrm{cm\,s^{-1}}$). Only subsurface passages in rises and ridges that subdivide ocean basins (**Figure 1**) seemed to allow for more energetic deep interior currents funneling through gaps and channels.

Until a few decades ago practically all knowledge about abyssal currents had to be inferred from the

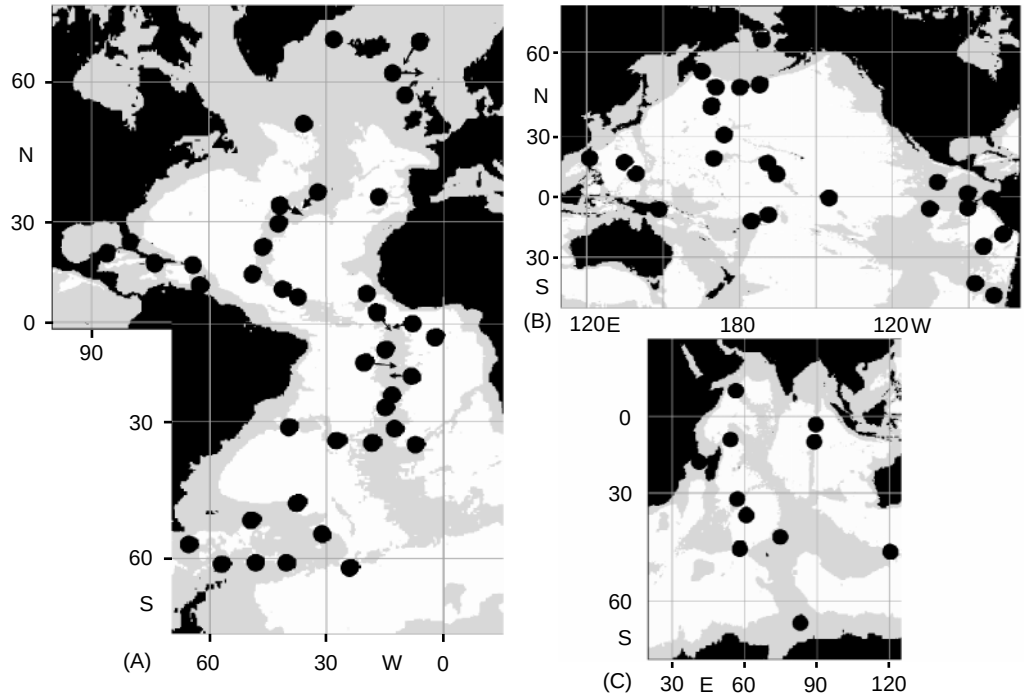

Figure 1 Major subsurface fracture zones, passages, and sills of the world's ocean. (A) Atlantic, (B) Pacific, (C) Indian Ocean. These topographic features represent important constraints for deep and bottom water spreading paths (after http://www.soc.soton.ac.uk/JRD/OCCAM/sills.html).

perspective of property fields like potential temperature, salinity, or potential density. Since these fields seem to be much more stable than velocity fields this method still yields reasonable general large-scale flow patterns even with scarce and nonsynoptic data sets. However, for any resolution beyond the low-frequency band of the current spectrum direct current observations by floating objects, moored instruments, or remotely measuring methods are essential.

In low latitudes of all oceans the permanent presence of the enormous, almost invariant temperature gradient between the surface at $> 25^{\circ}C$ and the floor at $< 2^{\circ}C$ requires a deep advection of cold water. The latter circulates freshly ventilated cold water from polar latitudes towards the Equator. For reasons of continuity a compensating poleward flow of water heated from the surface through the thermocline must occur above the abyssal layer of the tropics and the subtropics. Hence, the cold water drift propelled by sinking of cooled water masses (convection in selected areas) accelerates an endless global circulation cell known as the meridional overturning circulation (MOC), occasionally called the global conveyor belt (**Figure 2**). Its bottom-nearest limb, and sometimes also one or two layers in motion above it are characterized by the abyssal circulation.

The Stommel-Arons Concept and Diffusivity in the Interior

The concept that rising water from a flat deep-sea bottom without density stratification has to be replaced by convectively formed water is a key element of the modern Stommel-Arons theory of abyssal circulation. While the freshly ventilated water sinks in only a few selected semi-enclosed polar regions, the rising process itself occurs over broad lateral scales everywhere at lower latitudes. As a consequence it is possible to distinguish between two different dynamical regimes of the abyssal circulation (**Figure 3**). (1) A small (typically only 100–200 km wide) corridor at the continental rises and near the slopes on the western margins of the ocean's basins is occupied by deep western boundary currents (DWBCs). (2) The huge remaining interiors of the basins, fed laterally by DWBCs, are ruled by a uniform broad-scale upwelling regime. The inherent vertical velocities imply vortex stretching on top of the abyss. Conservation of potential vorticity then requires the poleward return drift in the interior.

Not long after the concept of DWBC was hypothesized in 1958, the first observations confirming its existence were made beneath the Gulf Stream in the north-western Atlantic using neutrally buoyant

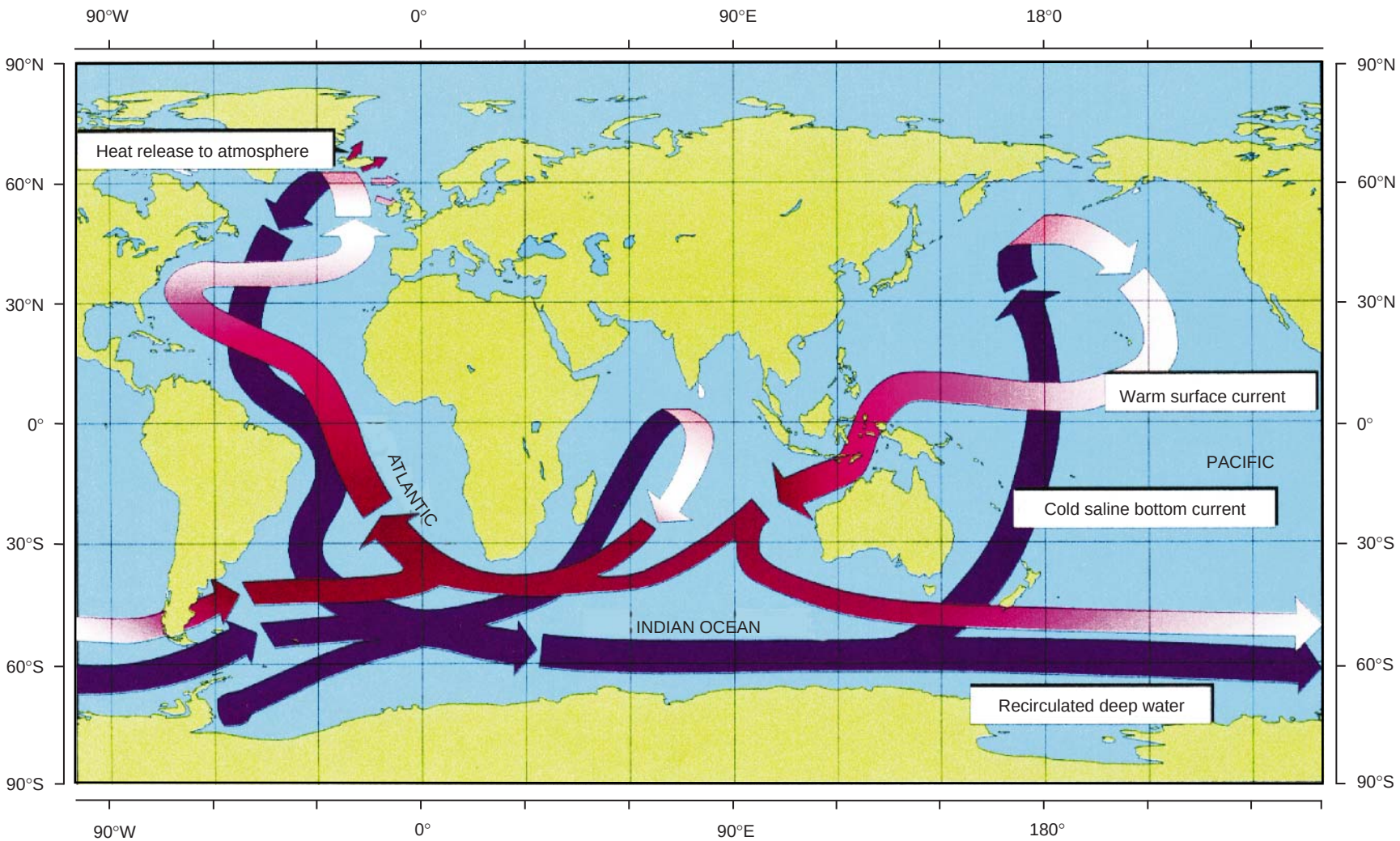

Figure 2 The Atlantic thermocline circulation as a key element of the global oceanic circulation. (After Broecker (1991), modified by Meier-Reimer.)

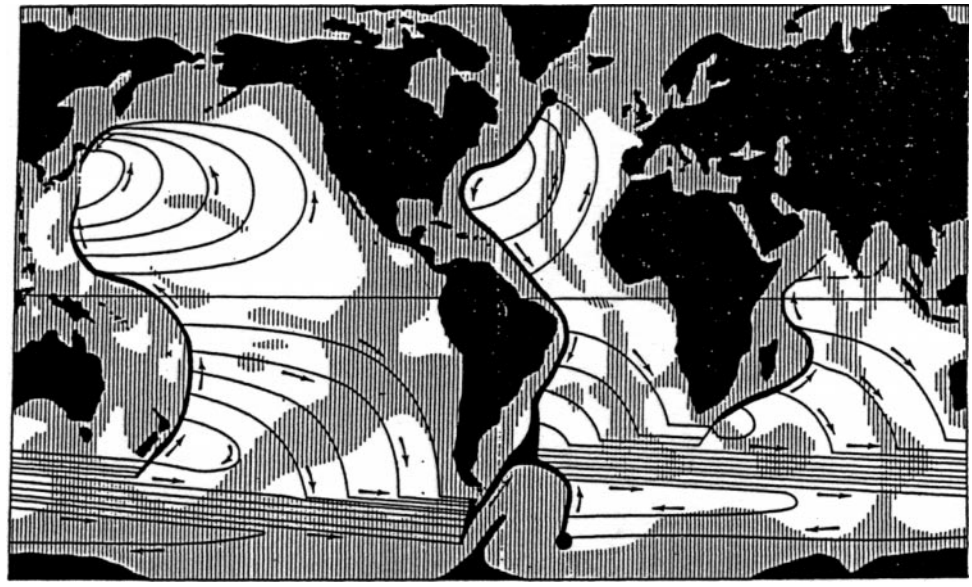

Figure 3 The Stommel-Arons (1958) concept of the abyssal circulation in the Atlantic. A system of western boundary currents feeds a slow broad-scale upwelling regime in the remaining interior of the basins. (Reprinted from *Deep-Sea Research* 5, Stommel H, The abyssal circulation, pp. 80–82, Copyright (1958), with permission from Elsevier Science.)

Swallow floats. Shortly afterwards, the newly detected deep equatorward drift led to a supplementary experiment to find the slow poleward countercurrent of the interior flow. The test failed at the time (1962) in so far as no flow with a slow, persistently northward velocity component could be proved. Instead, the mesoscale eddy phenomenon at great depths was discovered.

In steady state the vertical flux of heat at the base of the thermocline in lower latitudes can be formulated as the balance of temperature advection and its vertical diffusion:

$$\vec{u}\cdot\nabla T + w\frac{\partial T}{\partial z} = k\frac{\partial^2 T}{\partial z^2} \qquad [1]$$

where $\vec{u}$ is the lateral current vector, T temperature, w vertical velocity component, z vertical coordinate, and k eddy diffusivity. This temperature equation implies for the interface between the base of the thermocline and the top of the abyss the generation of a vertical velocity to balance the upwelled cold water and the downward diffusion of heat. An assumed sinking rate of $20\times10^6\,\mathrm{m^3\,s^{-1}}$ in high latitudes and an active lower thermocline interface of $3\times10^8\,\mathrm{km^6}$ yields a global integral upwelling speed of $\mathrm{O}(0.1\,\mathrm{dm\,d^{-1}})$. An adjoined downward diffusion with a diffusivity of $\mathrm{O}(1\,\mathrm{cm^2\,s^{-1}})$ can be estimated under the assumption of a vertical scale of 1 km within the abyssal upwelling regime. **Figure 4** depicts a sketch of the integrated form of [1] under the assumption of negligible lateral currents along isotherms.

$$w\cdot T = k_d\frac{\partial T}{\partial z} \qquad [2]$$

where k_d is the cross-isothermal diffusivity.

Observations of k_d are difficult to conduct. On a global scale numerical values of k_d fluctuate in a wide range (1–$500\,\mathrm{cm^2\,s^{-1}}$). A summary of the available sparse estimates from the Atlantic is reproduced in **Figure 5**.

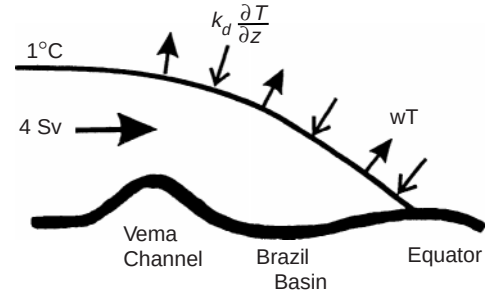

Figure 4 Schematic representation of eqn [2], the balance of downward diffusivity and upwelling across the 1°C isotherm level of the western South Atlantic. (After Hogg *et al.*, 1994 © Springer Verlag.)

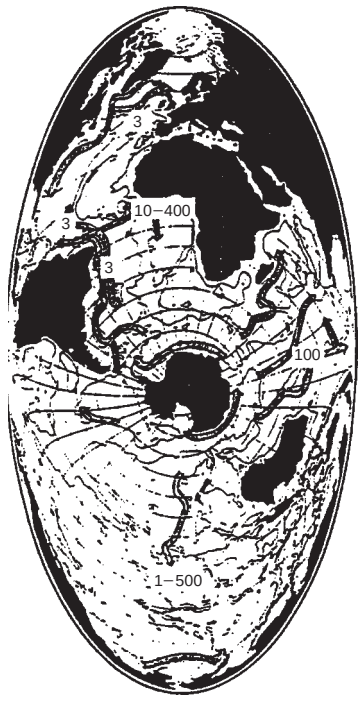

Figure 5 Some estimates of cross-isotherm diffusivity in $cm^2\,s^{-1}$ in the abyss of the world's oceans. (After Hogg, 2001, © Academic Press.)

Figure 6 gives a rare example of the heterogeneity of cross-isopycnal diffusivity in the interior Brazil Basin. The diffusivity is quantified from uniform microstructure observations at all depths above the smooth abyssal plains and west of the Mid-Atlantic Ridge. Estimates range from very weak ($<0.1\,cm^2\,s^{-1}$) to moderate ($>5\,cm^2\,s^{-1}$) turbulent signals. The latter enhancement is observed above the rough flanks of the ridge. The response is especially prominent within 500 m above the bottom.

The abyss contains recirculation cells. Significant amounts of cold water do not participate directly in the global meridional overturning cell. They circulate horizontally in response to the upwelling process. Such basin-wide recirculation cells (**Figure 7**) are distinctly influenced by the local bottom topography. Their persistence remains widely unexplored.

In summary, it is of considerable interest to quantify rates of sinking waters in high latitudes because the compensating abyssal upwelling is believed to drive the internal horizontal circulation of the oceans.

Sources of Abyssal Waters

Figure 8 represents a refined global update of the highly schematized deep Atlantic circulation pattern in **Figure 3**. Antarctica lies in the center. The North Pole cap is split; it is situated towards the outer edges of the Pacific and Atlantic blocks. All three oceans are interconnected by the Southern Ocean as the circum-Antarctic water ring is called. In this strongly simplified pattern of the global water mass circulation the abyss ranges from the lower third of the displayed water column down to the seafloor.

Regions of sinking waters are symbolized in **Figure 8** by near-surface downward arrows. They are unevenly distributed in both hemispheres. In fact, they are limited to the Antarctic Circumpolar Current System (ACCS) and to the high latitudes of the North Atlantic. In addition to bottom and deep water sources there are contributions from outflows of marginal seas (not shown in **Figure 8**). Although these flows reach only intermediate depth levels they affect characteristic water masses of the abyss beneath their own spreading level.

Several discrete locations for water sinks have been identified around Antarctica. Completely homogenizing wintertime convection down to the bottom of this semi-enclosed basin was observed only in Bransfield Strait south of the South Shetland Islands. However, in all other locations around Antarctica cooled and freshly ventilated water sinks to the bottom where it behaves like a contour current on the rotating earth. These densest waters in thin layers on the bottom mix with surrounding slightly warmer water masses and finally are transformed into Antarctic Bottom Water (AABW) spreading equatorward in all oceans. Known sinking areas are the Weddell Sea, Ross Sea, Wilkes-Adélie Coast, and some locations off Enderby Land and the Prydz Bay.

Because the generation of AABW is characterized by highest densities (due to the freezing temperatures in the source regions), AABW can be detected by low (potential) temperature signals close to the bottom everywhere in the Southern Hemisphere and in lower latitudes of the Northern Hemisphere. **Figure 9** demonstrates the global deep flow at 4000 m inferred from temperature distribution in the world ocean. The main production regions of sinking waters in the Weddell Sea (and near Iceland in the Northern Hemisphere) are labeled by arrows.

The northern counterpart of AABW is called North Atlantic Deep Water (NADW). Since its potential density is slightly different than that of AABW both water masses create an abyssal stratification where they encounter. Formation areas of NADW are located in the Nordic seas, i.e. the Norwegian and Greenland Seas. Convectively formed deep water from polar regions spills through outflow channels over sills to the north west and south east of Iceland. The outflow products are

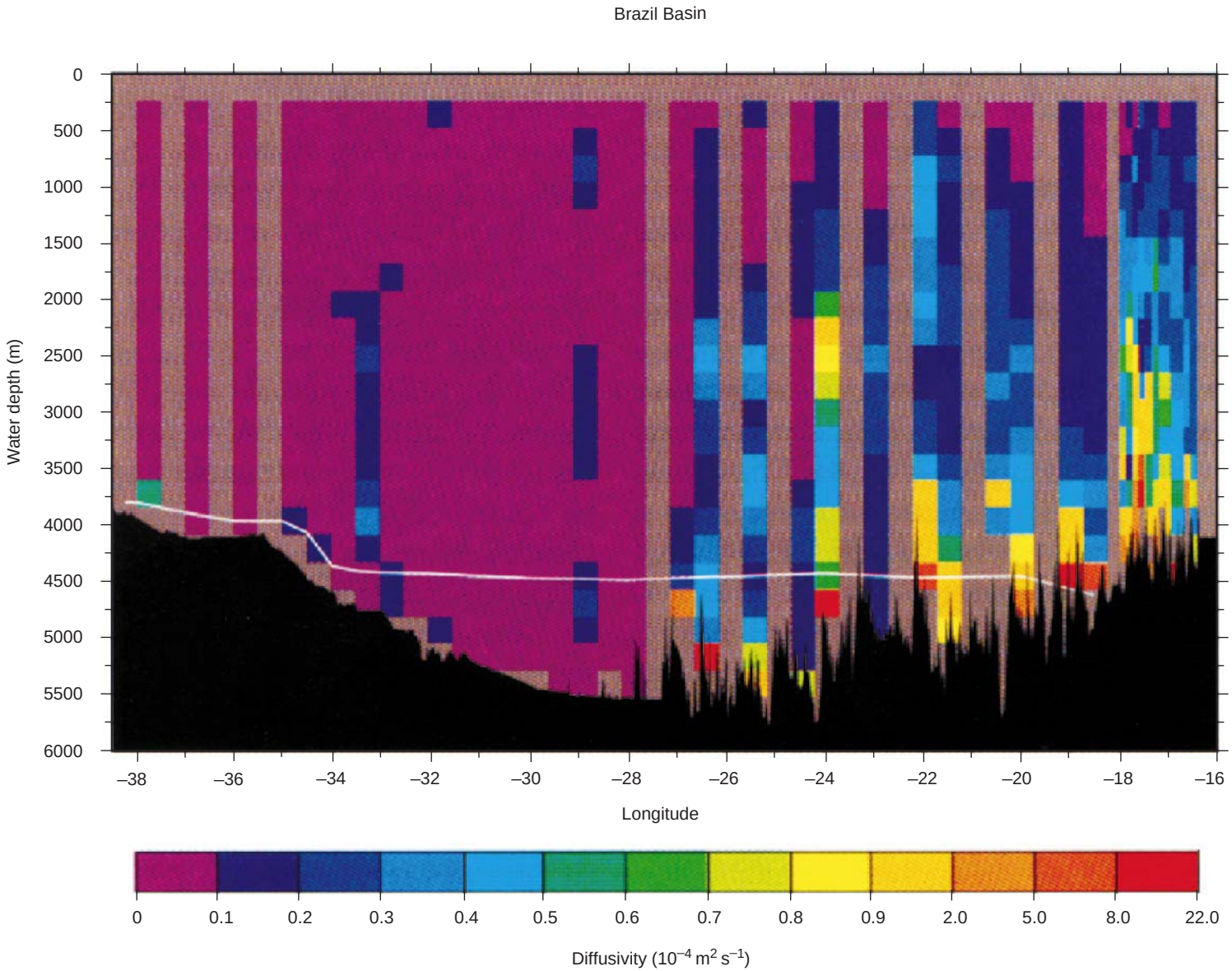

Figure 6 Directly observed distribution of diffusivity in the South Atlantic. The section covers the range between the continental rise off Brazil and the western flanks of the Middle Atlantic Ridge. Highest diffusivity values are correlated with the rough topography on the slopes of the ridge. (After Polzin *et al.*, 1997 © *Science.*)

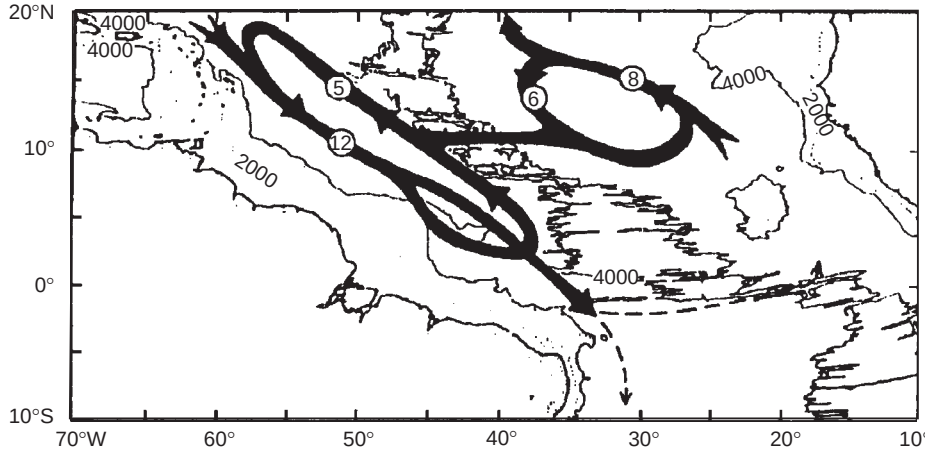

Figure 7 Example of abyssal recirculation cells in the tropical North Atlantic Ocean. Numbers indicate volume transports of lower North Atlantic Deep Water in $10^6\,m^3\,s^{-1}$. (After Friedrichs and Hall, 1993. Courtesy of the *Journal of Marine Research*.)

called Denmark Strait and Iceland Scotland Overflow Waters. On their way into the subpolar North Atlantic, the swift overflow plumes with speeds exceeding $50\,cm\,s^{-1}$ are subject to strong topographic control along the slopes of Greenland and the Mid-Atlantic Ridge, respectively. The high propagation speed of overflow waters favors further transformations by entrainment from intermediate waters increasing its transport rate in selected regions by a factor of 2 or more (**Figure 10**).

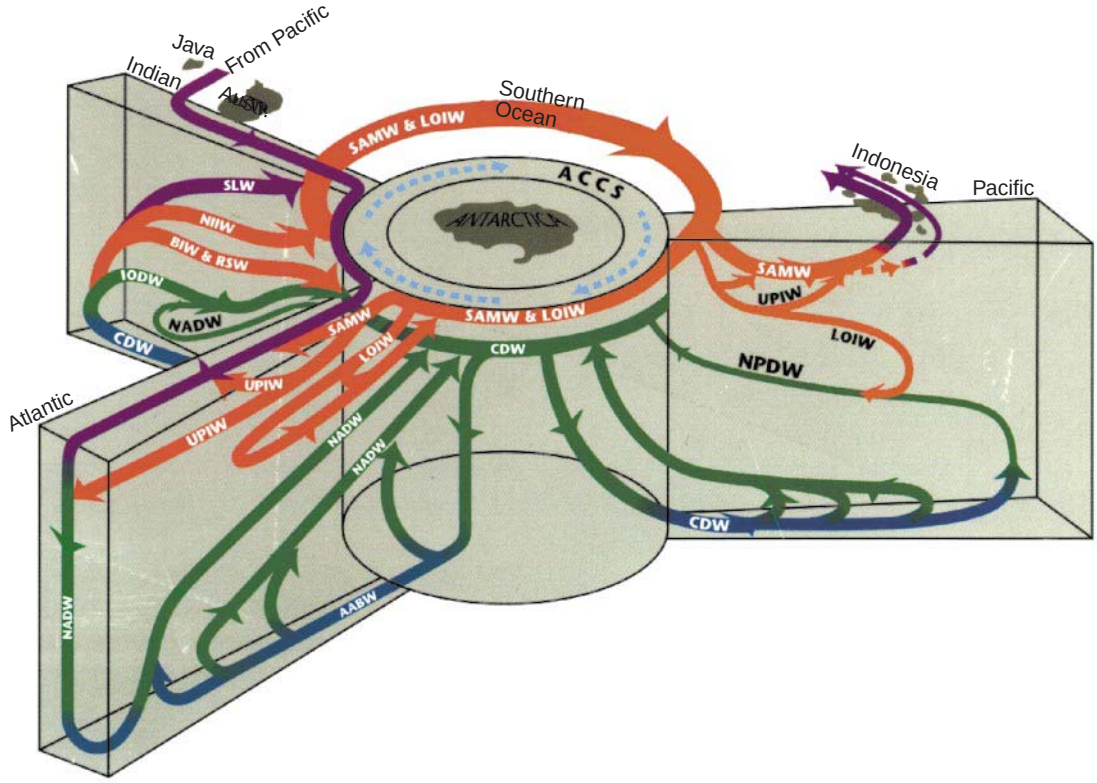

Figure 8 The complex global circulation. Colors: red and purple, thermocline waters; green and blue, abyssal waters. For details see text. Abbreviations: SAMW, SubAntarctic Mode Water; LOIW, Lower Intermediate Water; SLW, Surface Layer Water; UPIW, Upper Intermediate Water; NIIW, North-west Indian Intermediate Water; BIW, Banda Intermediate Water; RSW, Red Sea Water; CDW, Circumpolar Deep Water; NADW, North Atlantic Deep Water; NPDW, North Pacific Deep Water; IODW, Indian Ocean Deep Water; AABW, Antarctic Bottom Water. (Reproduced with permission from the Woods Hole Oceanographic Institution, Schmitz 1996a, 1996b.)

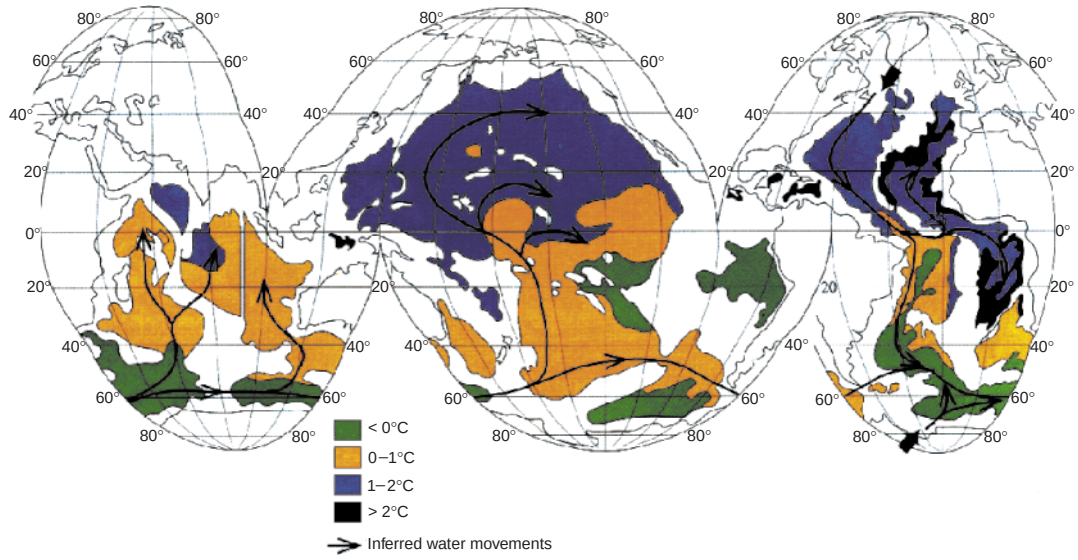

Figure 9 Global near-bottom potential temperature distribution and inferred flow paths of abyssal waters at 4000 m depth. (Reproduced with permission from an article by Charnock, The Atmosphere and the Ocean; in Summerhayes CP and Thorpe SA, *Oceanography, An Illustrated Guide* © 1996 Manson Publishing.)

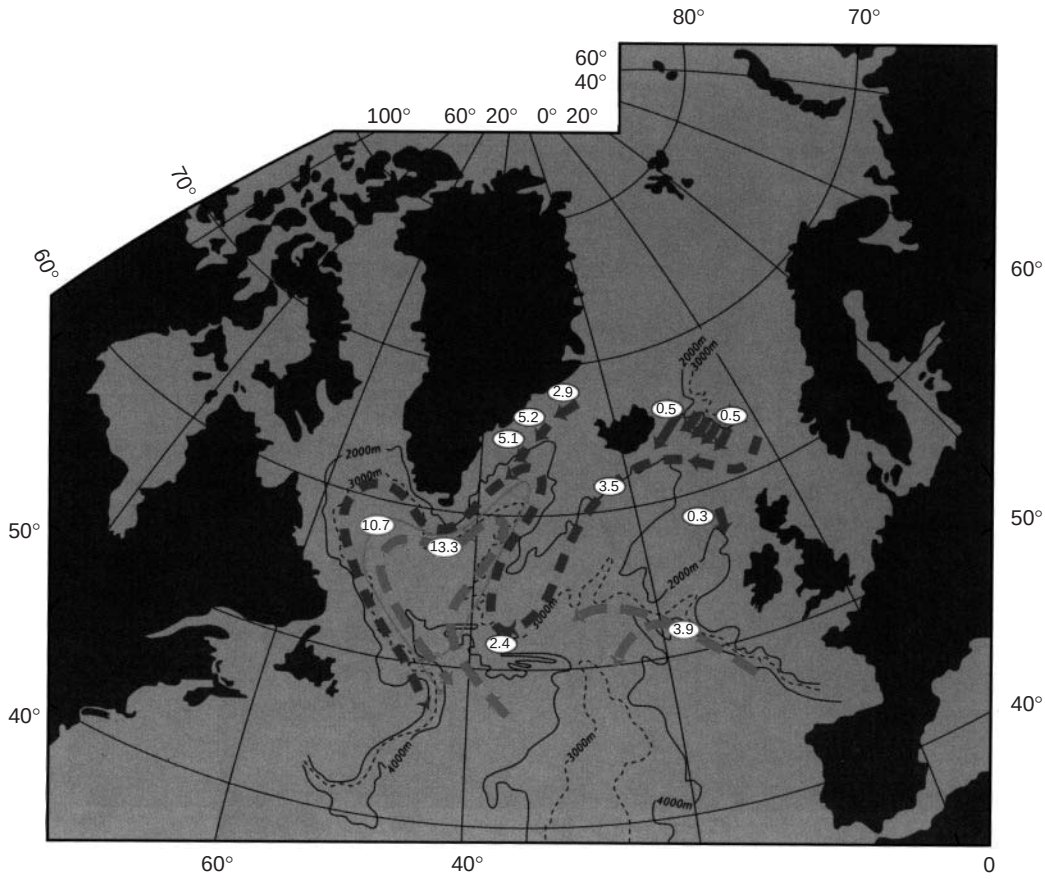

Figure 10 Examples of deep entrainment from the subpolar North Atlantic. Numbers represent volume transports in $10^6\,m^3\,s^{-1}$. Note the observed significant increase of transport along the east Greenland side which is caused by Denmark Strait Overflow Water. The Denmark Strait between Iceland and Greenland is also called Greenland Strait. (Reproduced with permission from Dickson RR and Brown J, *Journal of Geophysical Research* 99, 12319–12341 (1994) © American Geophysical Union.)

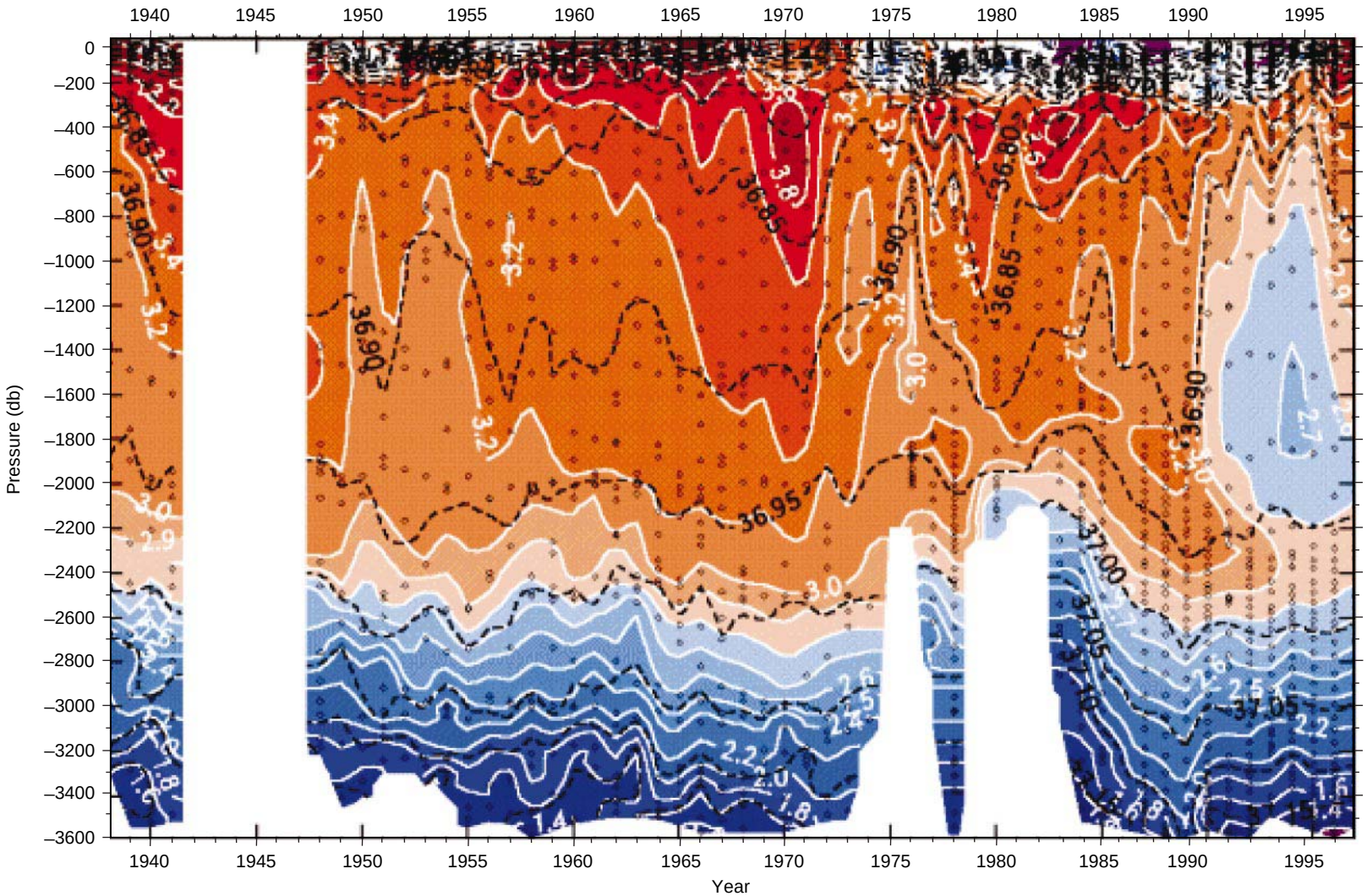

Figure 11 Demonstration of interannual variability (1938–97) of potential temperature in °C (colors and white isotherms) and potential density $\delta_{1.5}$ (kg m^{-3} (dashed black lines) referenced to 1500 dbar pressure level. (After I Yashayaev *et al.*, www.mar.dfo-mpo.gc.ca/science/ocean/woce/absea/labsea_poster.html.)

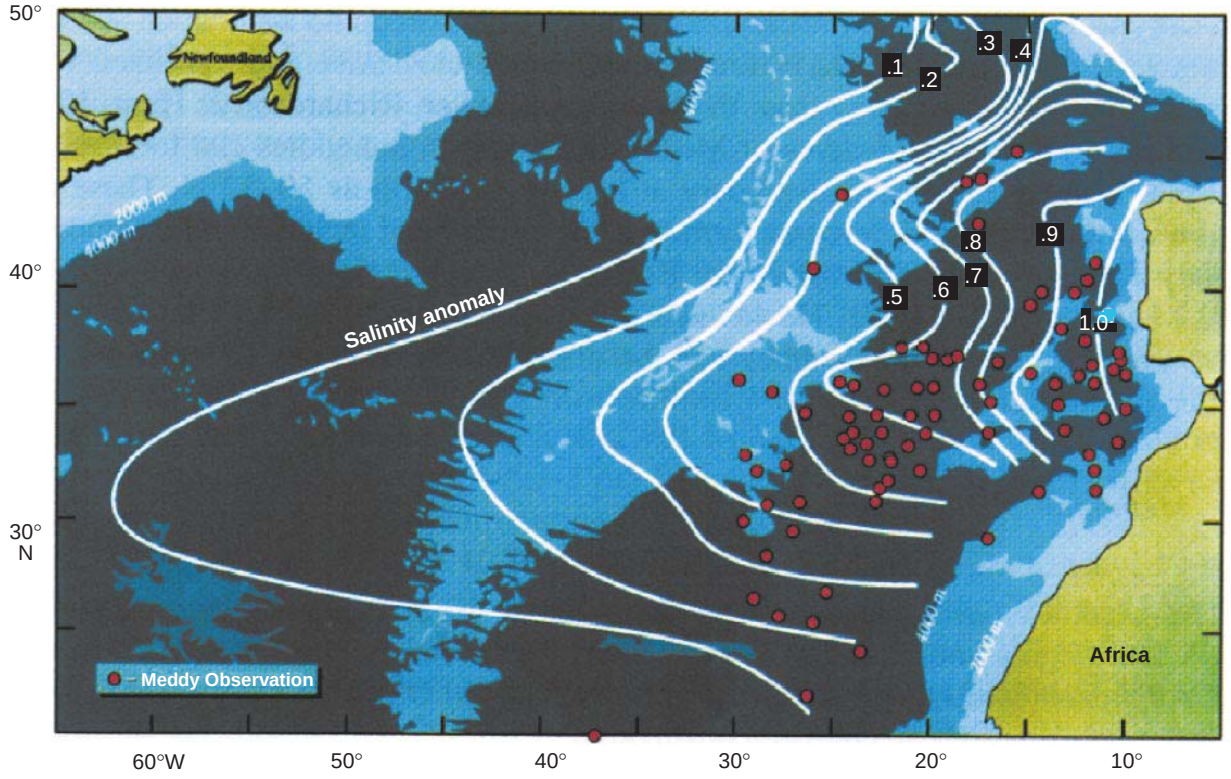

Figure 12 Influence of the Mediterranean Water on the salinity distribution at 1100 m of the North Atlantic. Isohalines represent positive anomalies relative to 35.01. Circles depict observed high salinity eddies of Mediterranean Water (Meddies). (Reprinted from *Progress in Oceanography* 4, Richardson PL, Bower AS and Zenk W, A census of meddies tracked by floats, pp. 209–250 © (2000) with permission from Elsevier Science and the American Meteorological Society.)

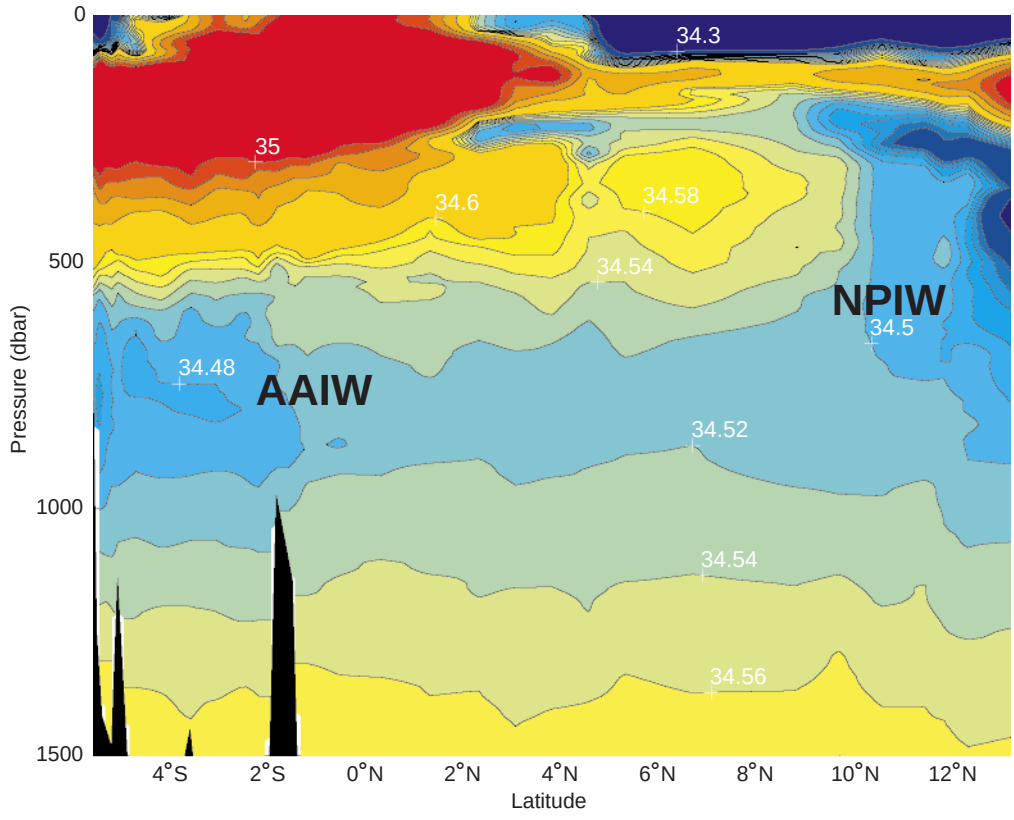

Figure 13 Salinity distribution (PSU) of Antarctic and North Pacific Intermediate Waters in the tropical western Pacific along 150°E. (After Holfort and Zenk, 1999.)

Additional mixing occurs with seasonally generated Labrador Sea Water. The latter also is formed by deep wintertime convection; its seasonal generation rate fluctuates substantially on interannual scales (**Figure 11**).

Local formation regions are not restricted to the western and central Labrador Sea itself. The western Irminger Sea seems to contribute to NADW formation as well.

Formation and sinking rates due to deep convection of AABW around Antarctica and of NADW in the North Atlantic are about equal in volume. Each hemisphere contributes $\sim 10 \times 10^6\,\mathrm{m^3\,s^{-1}}$. In the Southern Ocean generation sites are less focused compared with the Nordic Seas of the Atlantic. In the Pacific and Indian Oceans northern sources of abyssal waters are unknown (or at least are insignificant in the Pacific).

Overlying waters from two additional sources influence the abyssal circulation. (1) The excess evaporation over precipitation in the Mediterranean and Red Seas increases salinities and densities of these marginal seas substantially in comparison with the adjacent oceans. These density differences force exchange currents in the connecting straits (Strait of Gibraltar and Bab-el-Mandeb). The outflows sink to their equilibrium levels where they form pronounced intermediate high salinity layers in the North Atlantic (**Figure 12**) and northern Indic, respectively. (2) In selected regions of the southern polar frontal zone notable amounts of low salinity Antarctic Intermediate Water (AAIW) downwell and become part of the intermediate circulation. AAIW is found northward of subpolar regions in all three oceans. In the Pacific there is also a northern mode of intermediate water which is called North Pacific Intermediate Water (**Figure 13**).

Deep Western Boundary Currents (DWBC)

In contrast to the slow interior drift in ocean basins DWBC are much easier to access by direct observations. They can be revealed by property characteristics of parameters like temperature, salinity, nutrients or other chemical tracers, or be quantified by moored instrumentation. Following the schematic circulation diagram (**Figure 8**) we expect three stacked opposite DWBC cores at intermediate and abyssal levels in the South Atlantic: northward propagating AABW with mixing components of Circumpolar Deep Water and of the Weddell Sea Deep Water, southward-flowing NADW at least reaching the southern rim of the subtropics, and AAIW with a northward drift again. Water mass distributions

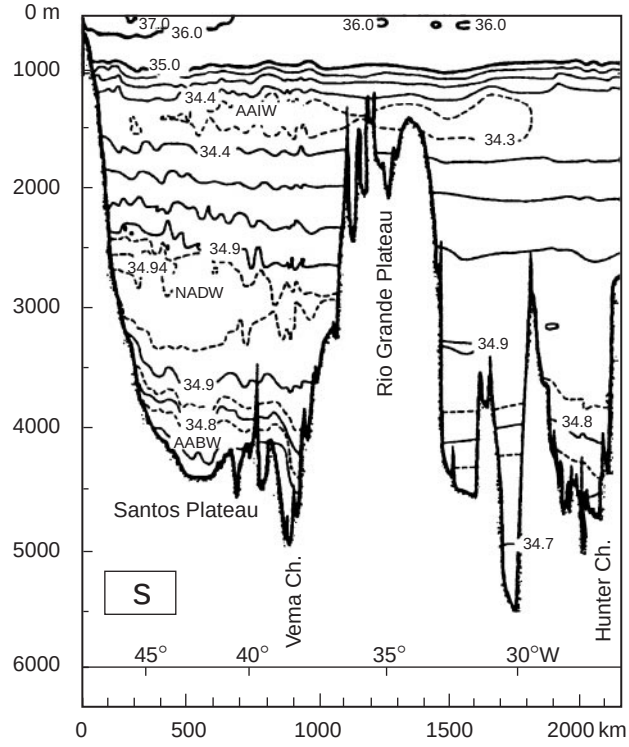

Figure 14 Salinity distribution (PSU) on a section across the Rio Grande Rise, South Atlantic, at nominally 30°S between the slope off Brazil and the Middle Atlantic Ridge. The Vema and Hunter Channels allow an active equatorward flux of Antarctic Bottom Water (AABW). More saline North Atlantic Deep Water (NADW) is advected poleward above the bottom water. On top of the abyssal layers lower saline Antarctic Intermediate Water (AAIW) again spreads equatorward. (Reproduced with permission of the American Meteorological Society from Hogg *et al.*, 1999.)

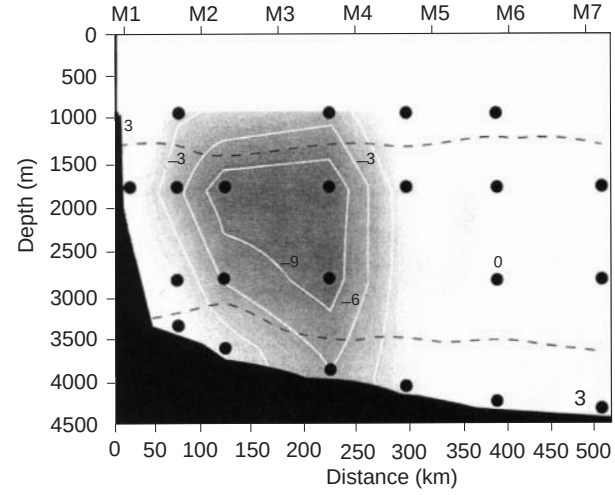

Figure 15 Eulerian long-term observation of the southward-flowing North Atlantic Deep Water at nominally 18°S. Isoclines of current speeds in $\mathrm{cm\,s^{-1}}$. The prime deep western boundary current of Antarctic Bottom Water is pressed against the continental slope off Brazil. Dashed lines denote the conventional upper and lower boundaries of NADW. (Reproduced with permission of the American Meteorological Society from Weatherley *et al.*, 2000.)

and their dynamical imprints are exemplarily displayed in form of a hydrographic section across the Rio Grande Rise at $\sim 30^{\circ}$S. This ridge separates the abyssal Argentine from the Brazil Basins (**Figure 14**). Long-term current observations with moored instruments farther north at 18°S are reproduced in **Figure 15**.

The core of the southward flowing NADW with averaged speeds of $> 10\,\mathrm{cm\,s^{-1}}$ is centered at 2200 m about 200 km offshore. The integrated transport of the NADW plume amounts to $39 \times 10^6\,\mathrm{m^3\,s^{-1}}$. The deepest northward AABW component along the continental rise with long-slope speeds of $< 3\,\mathrm{cm\,s^{-1}}$ is less developed.

The most recent transport estimates within the AABW from the Atlantic are shown in **Figure 16**. The northern part of this graph is shown in more detail in a schematic diagram jointly with lower NADW invading the Sargasso Sea and adjacent regions from the northern end of the Americas (**Figure 17**).

Mixing of both abyssal water masses is symbolized by stars in **Figure 17**. The NADW drift grows from $\sim 13 \times 10\,\mathrm{m^6\,s^{-1}}$ south of the southern tip of Greenland (Cape Farewell) to $\sim 40 \times 10^6\,\mathrm{m^6\,s^{-1}}$ off the Caribbean island arc.

In contrast to the Atlantic the basin-wide spreading of abyssal waters in the Pacific is exclusively controlled by the Antarctic Circumpolar Current System (ACCS). The lowest stratum is filled with Circumpolar Deep Water (CDW), a mixture of converted AABW and transformed NADW, possibly homogenized by repeat circulation in the Southern Ocean. Potential temperatures of CDW at 32°S range from 0.6 to 1.2°C. It enters the South Pacific as a DWBC and returns to the ACCS as Pacific

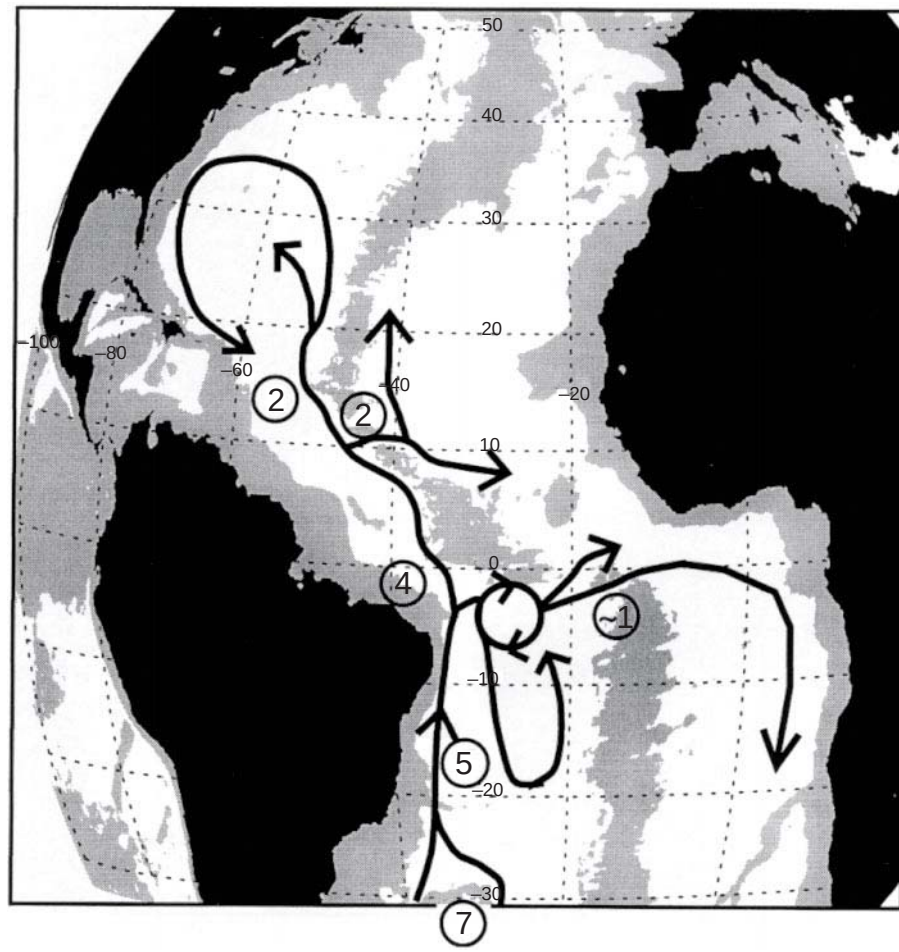

Figure 16 Spreading paths of Antarctic Bottom Water in the Atlantic after miscellaneous observations. Numbers indicate volume fluxes in $10^6\,\mathrm{m^3\,s^{-1}}$. Originally the AABW spreading path is restricted to the western side of the South Atlantic. It enters the subtropical region through the Vema and Hunter Channels at 30°S. The eastern basin is only accessible via the Vema Fracture Zone (11°S) and through the Romanche and Chain Fracture Zones near the equator. (Reproduced with permission of the American Meteorological Society from Stephens and Marshall, 2000.)

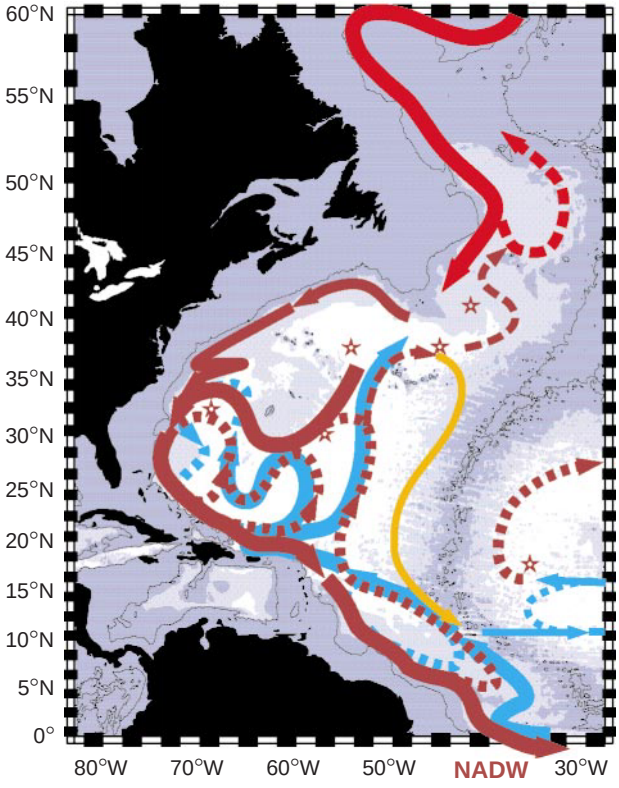

Figure 17 The complex abyssal circulation in the western North Atlantic. Colors: red and brown, flow of North Atlantic Deep Water; blue, Antarctic Bottom Water. Dashed lines indicate conceivable recirculation branches. Stars denote regions of abyssal entrainment. (Reproduced with permission from McCartney and Curry, 2001.)

Deep Water (PDW) after internal mixing and upwelling decades or centuries later.

The region north east of northern New Zealand delineates the gateway for CDW into the south-east Pacific Basin (**Figure 18**). Its boundary current system was found from 2-year long observations to be $\sim 700\,\text{km}$ wide. The maximum mean velocity of the applied current meter array was $9.6\,\text{cm}\,\text{s}^{-1}$ on the eastern flank of the Tonga-Kermadec Ridge. The time-averaged transport amounts to $15.8 \times 10^6\,\text{m}^6\,\text{s}^{-1}$ with a standard error of $9.2 \times 10^6\,\text{m}^6\,\text{s}^{-1}$ for the focused northward advection of the CDW core.

A striking aspect of the overall observations at 32°S are the total transport (CDW plus PDW) fluctuations ranging from $(-17$ to $+51) \times 10^6\,\text{m}^6\,\text{s}^{-1}$, typically oscillating over periods of a few months with amplitudes of 1–2 times the mean.

About 20° farther north the northward flow of CDW into the main basins of the Pacific is topographically controlled by the Samoan Passage. Recent observations with moored current meters have yielded northward transports of $10.6 \pm 1.7 \times 10^6\,\text{m}^6\,\text{s}^{-1}$ from an 18 month measuring program.

In accordance with the Stommel-Arons concept further decreases of DWBC transports were estimated at 10°N ($9.6 \times 10^6\,\text{m}^6\,\text{s}^{-1}$) and 24°N (($4.9$ and $9.1) \times 10^6\,\text{m}^6\,\text{s}^{-1}$) from snapshot hydrographic surveys (**Figure 19**).

To date estimates of the returning PDW transports are rare and quantitatively inconsistent.

The abyssal conditions of the Indic resemble those of the Pacific: no deep convective sources in the north are available (**Figure 8**). Instead, the deep Indian Ocean is controlled by deep and bottom waters from the ACCS (CDW) with a particular influence from the southern South Atlantic (NADW). The Indonesian passages are too shallow to affect the Indic abyss immediately.

The topography of the Indic is different to that of the other oceans. Several meridionally aligned ridges divide this ocean into sub-basins. The pathways of deep flows are therefore more complex then assumed in the simple approach by the Stommel-Arons concept. **Figure 20** displays the distribution of water density, referenced to 4000 dbar at the bottom of the Indic. The graph enables a view of large-scale bottom water spreading on the base of hydrographic observations.

Three major inlets for deep water (CDW or modified NADW) are obvious at the northern tips of the Mozambique (38°E) and the Crozet (60°E) Basins. The spreading into the Australian Basin (125°E) is constrained by the Australian–Antarctic Discordance at 50°S, 123°E. The near-Equator Somali and Australian Basins are only accessible for deep flows through the Amirante and the Diamartina Passages, respectively. Long-term transport estimates of CDW spreading are rare. They lie clearly below the $10 \times 10^6\,\text{m}^6\,\text{s}^{-1}$ range.

Conclusions

During the past experimental period of the World Ocean Circulation Experiment (1990–99) significant progress in understanding of the abyssal circulation has been achieved. Deep Western Boundary Currents have been quantified on virtually all rises along continents and parallel to meridionally aligned ocean ridges. Pathways and transports of Deep Western Boundary Currents (DWBCs) were identified and quantified mostly with moored current meter arrays. Today the concept of a quasi-steady mean deep circulation has been outdated. In view of the omnipresent eddy kinetic energy with surprisingly large fluctuations more observations on a wide scale of temporal and spatial scales from the

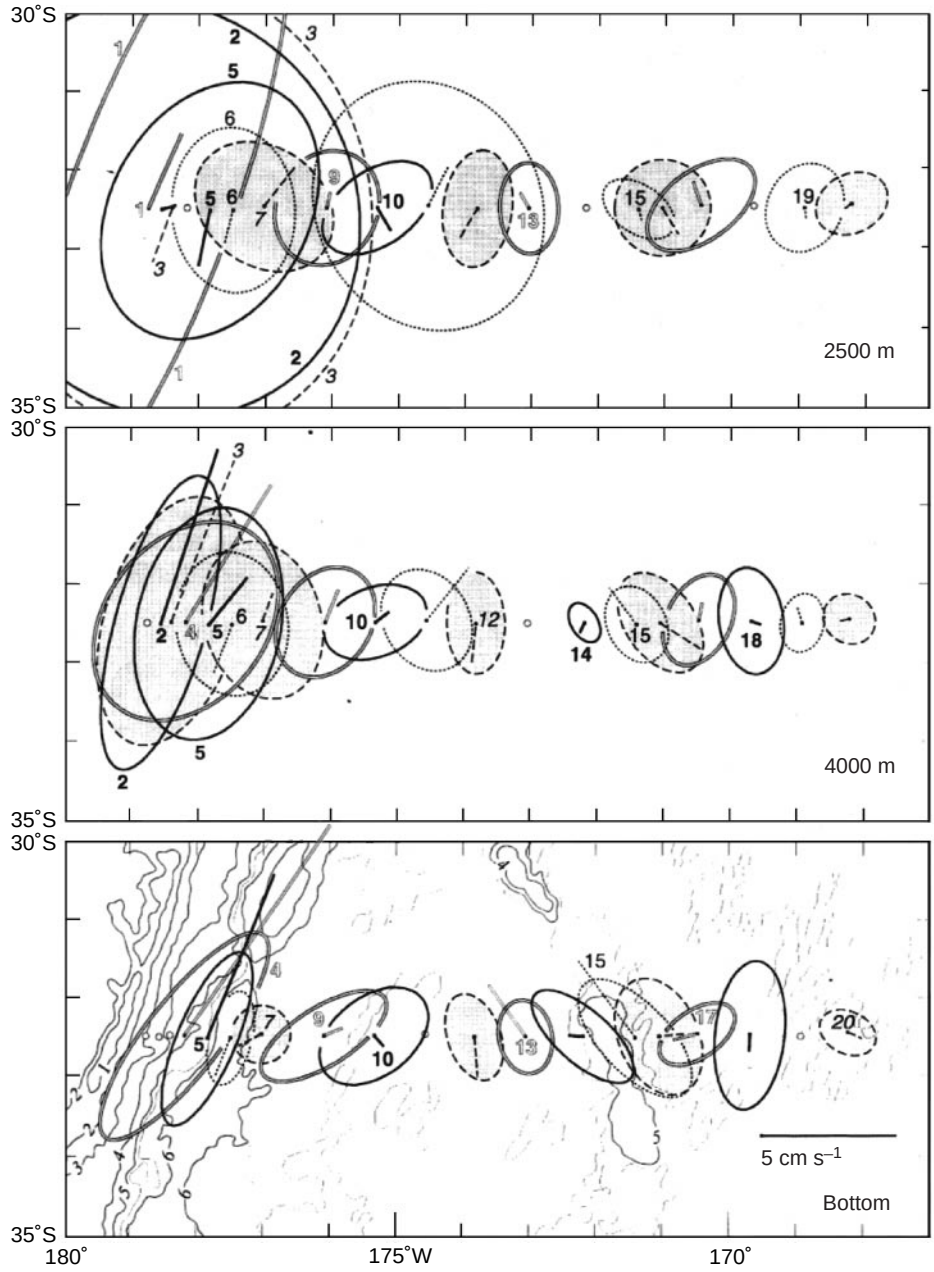

Figure 18 Long-term observations of the deep western boundary current system at 32°30′S at three instrumented abyssal layers (2500, 4000 m, near-bottom) of the Pacific. Mooring locations at dots are shown by the origin of the presented mean velocity vectors. Ellipses inform about the current's stability in form of the root mean square amplitudes. Small italics in the lower panel indicate depths in km. Bolder numbers are mooring identifiers. Note the clear bottom-intensified flow of Antarctic Bottom Water. The returning North Pacific Deep Water flow is less confined and highly variable. (Reprinted from *Progress in Oceanography* 43, Whitworth *et al.*, on the deep western-boundary current in the Southwest Pacific Basin, 1–54 © (1999) Elsevier Science and the American Meteorological Society.)

whole water column are essential. The need for long-term time-series in 'ocean observatories' has been recognized in international programs like the Climate Variability and Predictability Programme (CLIVAR) or the Global Ocean Observation System (GOOS).

The Stommel-Arons concept seems to be confirmed in respect to the balance of abyssal upwelling and downward heat flux through the base of the main thermocline. However, although the first Lagrangian vector time-series from the abyss of the Brazil Basin are now available, according to the

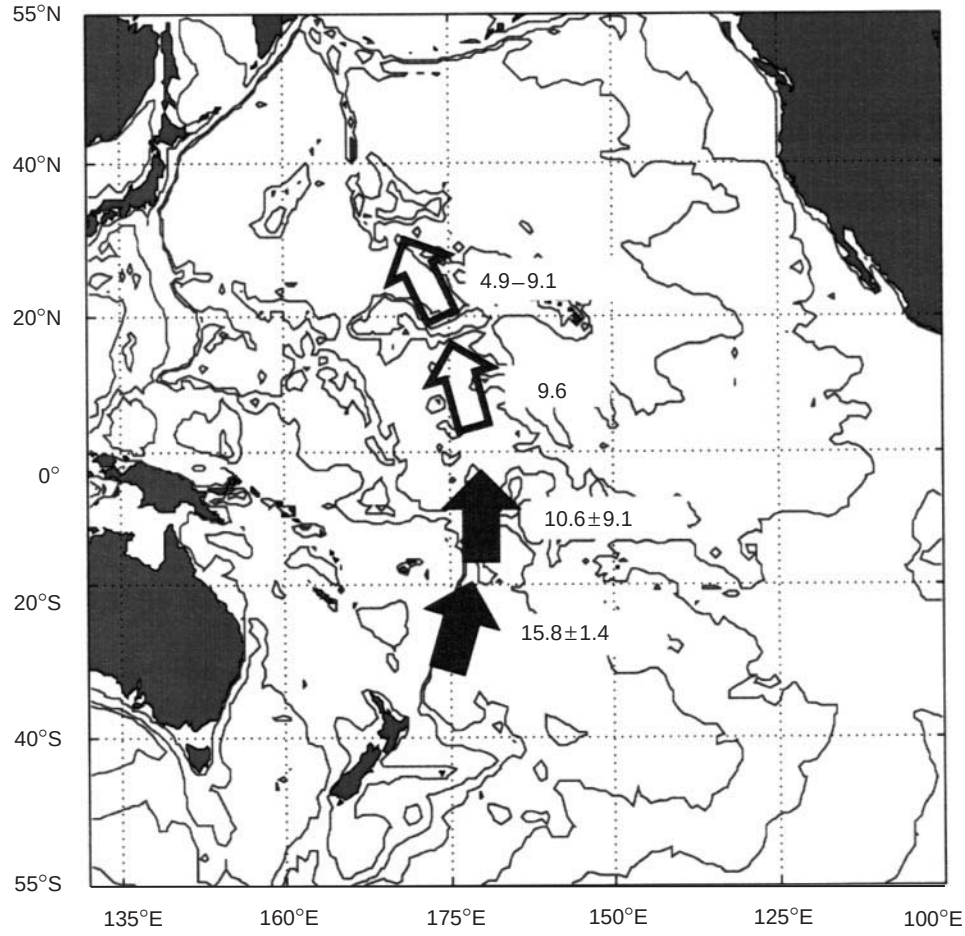

Figure 19 Inflow of Antarctic Bottom Water into the western basins of the subtropical/tropical Pacific. Heavy arrows were inferred from long-term current meter observations, open arrows represent single realizations from hydrography. Numbers indicate volumes of the deep western boundary current transports in $10^6 m^3 s^{-1}$ (After Hogg, 2001 © Academic Press.)

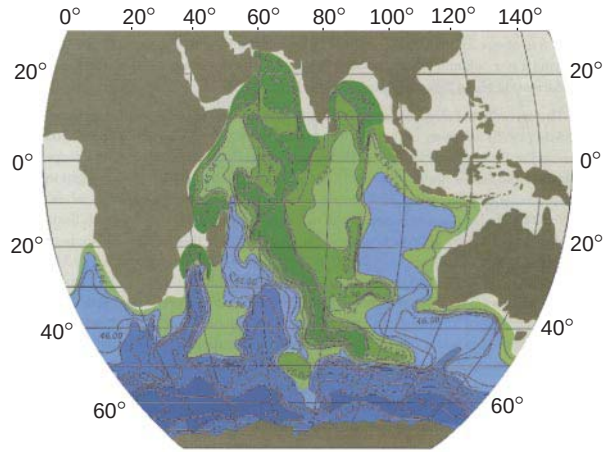

Figure 20 The distribution of potential density σ_4 in $kg\,m^{-3}$ referenced to 4000 dbar is used as a tracer for the spreading of Antarctic Bottom Water in the Indian Ocean. Note the three distinct tongues of dense water invading the Indian Ocean from the Southern Ocean. (Adapted from Mantyla AW and Reid JL, *Journal of Geophysical Research* 100, pp. 2417–2439 (1995) © by the American Geophysical Union and from Schmitz, 1996b.)

theory, the slow poleward return drift remains inaccessible to direct observations, as was found some 30 years ago in the deep Sargasso Sea. In contrast to expectations, net flow displacements in the Brazil Basin over 800 days indicate preferred zonal advection of bottom water partly in opposing directions (**Figure 21**).

Besides current meter moorings improved instrumental approaches with autonomous arrays of density recorders ('moored geostrophy') or acoustic ocean tomography at a basin-scale lie at the frontier of new technologies for future integral observations. Such methods attenuate eddy noise before data are recorded, and hence reveal motion characteristics that may be closer to robust circulation patterns.

Progress has also been made with respect to the experimental determination of abyssal diffusivities. Heat transports through deep passages appears to be significantly higher and steady compared with unconstrained areas. This implies enhanced mixing

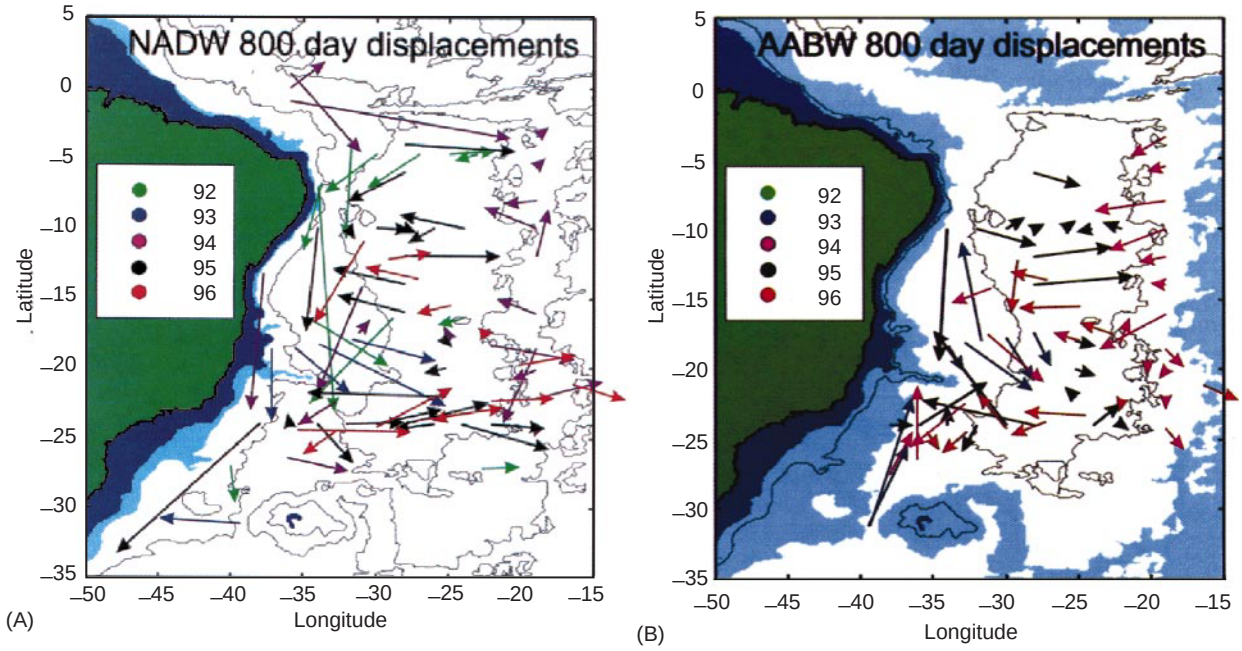

Figure 21 Displacement vectors from 800 days of the drift of North Atlantic Deep (A) and Antarctic Bottom Waters (B) in the Brazil Basin. Nominal observation levels were 2500 m (A) and 4000 m (B). Note the clear signal of boundary currents and the predominant zonal structure of the flow in the central basins. Numbers + 1900 indicate the years in which the Lagrangian current observations by neutrally buoyant floats were started. (From Hogg, 2001 © Academic Press.)

above passages converting them into important stirring agents of the abyss.

Finally, recirculation cells delineate a significant limb between the swift DWBC regime and the interior slow drift regions. These deep powerful current loops on a sub-basin-wide scale may explain the enormously high speed of the DWBC cores in lower latitudes, particularly in the Atlantic. Their variability strongly affects the meridional overturning cell and questions the role of the conveyor belt (**Figure 2**) in climate variability.

See also

Antarctic Circumpolar Current. Atlantic Ocean Equatorial Currents. Benguela Current. Brazil and Falklands (Malvinas) Currents. California and Alaska Currents. Canary and Portugal Currents. Current Systems in the Atlantic Ocean. Current Systems in the Southern Ocean. Deep Convection. Dispersion and Diffusion in the Deep Ocean. Double-diffusive Convection. East Australian Current. Florida Current, Gulf Stream and Labrador Current. Heat Transport and Climate. Kuroshio and Oyashio Currents. Non-rotating Gravity Currents. Open Ocean Convection. Overflows and Cascades. Pacific Ocean Equatorial Currents. Rotating Gravity Currents. Thermohaline Circulation. Water Types and Water Masses.

Further Reading

Broecker W (1991) The great ocean conveyor. *Oceanography* 4: 79–89.

Dickson RR and Brown J (1994) The production of North Atlantic Deep Water: Sources, rates and pathwalks. *Journal of Geophysical Research* 99: 12319–12341.

Friedrichs MAM and Hall MM (1993) Deep circulation in the tropical North Atlantic. *Journal of Marine Research* 51: 697–736.

Hogg N (2001) Deep circulation. In: Siedler G, Church J and Gould JW (eds) *Ocean Circulation and Climate*. London: Academic Press.

Hogg N, Siedler G and Zenk W (1999) Circulation and variability at the southern boundary of the Brazil Basin. *Journal of Physical Oceanography* 29: 145–157.

McCartney M and Curry R (2001) Abyssal potential vorticity in the western North Atlantic and the formation of Lower North Atlantic Deep Water. *Progress in Oceanography* (in preparation).

Mantyla AW and Reid JL (1995) On the origin of deep and bottom waters of the Indian Ocean. *Journal of Geophysical Research* 100: 2417–2439.

Pedlosky J (1979) *Geophysical Fluid Dynamics*. New York: Springer.

Polzin KL, Toole JM, Ledwell JR and Schmitt RW (1997) Spatial variability of turbulent mixing in the abyssal ocean. *Science* 276: 93–96.

Richardson PL, Bower AS and Zenk W (2000) A census of Meddies tracked by floats. *Progress in Oceanography* 4: 209–250.

Schmitz WJ Jr (1996a) *On the World Ocean Circulation: Some Global Features/North Atlantic Circulation*. 1, Woods Hole Oceanographic Institution, Technical Report, WHOI-96-03.

Schmitz WJ Jr (1996b) *On the World Ocean Circulation: The Pacific and Indian Oceans/A Global Update*. 2, Woods Hole Oceanographic Institution, Technical Report, WHOI-96-08.

Siedler G, Church J and Gould JW (eds) (2001) *Ocean Circulation and Climate*. London: Academic Press.

Stephens JC and Marshall DP (2000) Dynamical pathways of Antarctic Bottom Water in the Atlantic. *Journal of Physical Oceanography* 30: 622–640.

Stommel H (1958) The abyssal circulation. *Deep-Sea Research* 5: 80–82.

Summerhayes CP and Thorpe SA (1996) *Oceanography. An Illustrated Guide*. London: Manson Publishing.

Warren BA and Wunsch C (1981) *Evolution in Physical Oceanography*. The Massachusetts Institute of Technology.

Weatherly GL, Kim YY and Kontar EA (2000) Eulerian measurements of the North Atlantic Deep Water Western Boundary Current at 18°S. *Journal of Physical Oceanography* 30: 971–986.

Wefer G, Berger WH, Siedler G and Webb DJ (eds) (1996) *The South Atlantic: Present and Past Circulation*. Berlin: Springer-Verlag.

Whitworth T III, Warren BA, Nowlin WD Jr *et al*. (1999) On the deep western-boundary current in the Southwest Pacific Basin. *Progress in Oceanography* 43: 1–54.

ACCRETIONARY PRISMS

J. C. Moore, University of California at Santa Cruz, Santa Cruz, CA, USA

doi:10.1006/rwos.2001.0465

Introduction

Subduction of oceanic lithosphere along a convergent plate boundary transfers sediments and rocks from the underthrust lithosphere to the overriding plate, producing an accretionary prism. Accretionary prisms develop beneath the inner slopes of the deep ocean trenches that typically mark convergent plate boundaries. The subduction process destabilizes the mantle after about 100 km of underthrusting beneath the upper plate to produce magmas of the volcanic arcs that virtually always occur along convergent plate boundaries (**Figure 1**). As accretionary prisms grow through addition of oceanic material, they become coastal mountain ranges. When a continent collides with a subduction zone, the intervening accretionary prism becomes incorporated into the resultant great mountain belts. Thus, rocks in accretionary prisms sometimes are the only record of ancient vanished ocean basins. Accretionary prisms typically form on the upper plate of subduction zone thrust faults, which host the world's largest earthquakes. Because accretionary prisms incorporate soft sediments at high rates of deformation, they produce some of the world's most complexly deformed rocks, commonly called melanges. Sediments offscraped to form accretionary prisms are like sponges that yield fluids as they are squeezed and deformed during prism growth. The fluids affect the mechanics of faults; chemically dissolve, transfer, and deposit material; and support chemosynthetic biological communities. The shape of the accretionary prism is mechanically controlled by the strength of the material comprising the accretionary prism and its internal fluid pressure. At slightly fewer than half of modern convergent plate boundaries, accretionary prisms are not currently

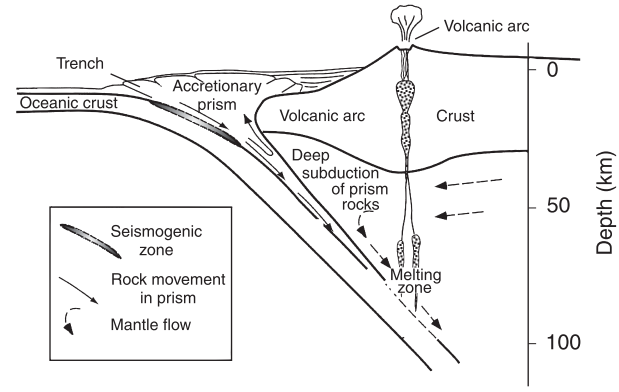

Figure 1 The setting of an accretionary prism in a generalized cross-section of a convergent plate boundary. Although the accretionary prism builds up primarily by scraping off material riding on the oceanic crust, some portions are deeply underthrust and flow back to the surface, while other portions are deeply subducted and participate in the formation of the igneous rocks of the volcanic arc.